Journal of Ceramic Processing Research. Vol. 21, No. 3, pp. 285~295 (2020)
(Received 25 June 2019, Received in revised form 16 September 2019, Accepted 26 September 2019)
https://doi.org/10.36410/jcpr.2020.21.3.285

J O U R N A L O F
Ceramic Processing Research

Effect of the ratio of eggshell and rice husk as starting materials on the direct synthesis of bioactive wollastonite by solid state thermal method

Sazia Sultana, Md. Maksudur Rahman, Zenefar Yeasmin, Samina Ahmed* and Farzana Khan Rony
Institute of Glass and Ceramic Research and Testing (IGCRT), Bangladesh Council of Scientific and Industrial Research (BCSIR), Dhaka-1205, Bangladesh

This paper describes the effect of the ratio of two starting materials, eggshell (ES, source of Ca) and rice husk (RH, source of silica) on the direct synthesis of wollastonite via a facile two-step solid state method, i.e. ball milling of the raw materials followed by calcination of the mixture at 1,000 ºC. The investigation was focused on optimizing the ratio of ES and RH to maximize the formation of wollastonite. Keeping the wt.% of RH constant, four different ratios of RH and ES (10:2.6, 10:3.0, 10:3.3 and 10:3.7) were used and the observed result revealed that the initial ratio of RH and ES plays a key role in controlling the formation of wollastonite as the major phase which was confirmed by x-ray diffraction (XRD) and Fourier Transform Infrared (FT-IR) techniques. The bioactive property of this wollastonite was studied in simulated body fluid at 37 ºC while the time dependent growth of hydroxyapatite (HA) on the surface of wollastonite was examined by SEM and XRD. Observed data supported the bioactive nature of wollastonite as biomaterial.

Key words: Wollastonite, Eggshell, Apatite, Bioactive.

Introduction

Wollastonite, a dazzling white to gray or brown coloured calcium meta silicate ($CaSiO_3$) has received enormous attention to the researchers. The application of wollastonite in traditional ceramics e.g. porcelain [1], heat insulating ceramics [2], concrete [3] and cement [4] is quite well known due to its various notable properties (fluxing characteristics, low shrinkage behavior and better strength). However, in the arena of advanced ceramics, pure wollastonite has been categorized as an innovative material which has proved its potentiality to be used as a bone regenerative bioceramic material [5] and presently it continues to be an eye-catching research field [6-11]. Furthermore, composite format of wollastonite, is also developed for biomedical applications [12]. However, the prime reason for the bioactivity of wollastonite, is the ability to form Si–OH bond on its surface upon exposure in simulated body fluid (SBF). Concerning the significance of wollastonite as biomaterial, researchers have already developed many routes, namely sol-gel [6, 9-11, 13-15], hydrothermal [16-18] solid state [19-21], ultrasonic irradiation [5] microwave assisted solid state [22] and wet chemical precipitation method [23] etc. to synthesize $CaSiO_3$. Being a non-toxic, solvent free and environment friendly method, hitherto, solid-state approach has ranked to be preferable.

Nevertheless, in addition to the synthesis route, the precursors used as calcium and silica sources are also important. Different combinations of the starting materials have been used by different researchers e.g. Udduttula et al. [6], Lakshmi et al. [9] and Wang et al. [13] used $[Ca(NO_3)]_2.\ 4H_2O$ and tetra ethyl orthosilicate (TEOS) as calcium and silica sources respectively; Anjaneyulu et al. [10] choice was eggshell and TEOS; eggshell and diatomite were chosen by Puntharod et al. [16] while snail shell and rice husk ash (RHA) were used by Phuttawong et al. [19]. The researchers of Vichaphund's group prepared wollastonite from eggshell and commercial grade (98%) silica [22]. In combination with $[Ca(NO_3)]_2.\ 4H_2O$ researcher also used $Na_2SiO_3.9H_2O$ as silica source [11]. However, researchers still continue to explore different combination of the raw materials to be used as the source of calcium and silica and numerous recipes used to synthesize wollastonite [24-36] are summarized in Table 1.

In this era of globalization, scientists across the globe are paying more and more attention to resolve environmental pollution problems and this has led them to be concerned in developing new synthetic routes as well as in utilizing waste materials. Keeping this view in mind, we have used waste ES (as Ca source) and RH (as silica source) together to synthesize wollastonite via solid state thermal treatment method.

RH, though categorized as waste/by-product but it contains cellulose (38.3%), hemicellulose (31.6%), lignin (11.8%) and silica (18.3%). Heat treatment or

*Corresponding author:
Tel : +8801817549816
Fax: +88-02-58613022
E-mail: shanta_samina@yahoo.com

Table 1. Summary of the recepies used to synthesize wollastonite by different methods.

Sl. No.	Precursor used as Ca and silica source	Method followed to synthesize wollastonite	Refs.
1.	ES and RHA	Sol-gel method	24
2.	ES and RHA	Sol-gel technique	25
3.	CaO and SiO_2	Sol-gel technique	26
4.	$Ca(OH)_2$ and Na_2SiO_3	Salt co-precipitation and subsequent thermal treatment	27
5.	Calcium nitrate and colloidal silica	Solution combustion	28
6.	Calcium nitrate and bentonite clay	Sol-gel technique	29
7.	Sea shell and float glass	Solid state reaction	30
8..	Limestone and rice husk ash (RHA)	Autoclaving technique	31
9.	CaO and soda lime silica glass	Conventional melt-quenching method	32
10.	Calcium oxide and rice husk	Autoclaving technique	33
11.	Calcium chloride and sodium silicate	Sol-gel and SPS techniques	34
12.	Limestone and silica sand	Solid state reaction	35
13.	Calcium carbonate, silica and nano silica	Hydrothermal synthesis	36

combustion of RH produces about 20-25 wt% of rice husk ash (RHA), which contains more than 90% silica. [37]. On the other hand, ES is enriched with $CaCO_3$ (94-97%) [38]. Hence these two agro-wastes are being getting the attention of the researchers to be used as the source of silica and Ca respectively in synthesizing biomaterials and or ceramic materials. Concerning the significance of RH and ES, to the best of our knowledge, for the first time, we have studied the effect of the ratio of ES:RH to synthesize $CaSiO_3$ even though individually either ES or RHA was used as calcium or silica source material in many previous studies [10, 16, 19, 22, 33].

Bangladesh is categorically considered as *Agriculture* or *Agro* based country having an annual production of 4-4.5 million metric tons (MT) of paddy which gives about 9.0 million tons of RH as waste product [39]. On the other hand, in Bangladesh the production of egg is 10168 million per annum [40] and consequently every year ~113000 tons of ES are thrown away to the environment. Hence, utilization of ES and RH will be beneficial in two ways: (i) synthesized wollastonite will be cost effective bioceramic material for biomedical applications, and (ii) it will be an effective material-recycling pathway for waste management.

Experimental Details

Materials and their processing

RH and ES were collected from rice mill and local restaurant and used as the source of silica and calcium respectively. Prior to using as source materials, RH was processed following a previously described method [13]. Briefly, RH was soaked in water for 5 minutes, maintaining the water to RH ratio at 20 L/kg. Then the mixture was kept undisturbed for couple of minutes to allow the unwanted materials to be settled down at the bottom. After that, RH was collected carefully from the upper portion of the mixture using a sieve of 60-mesh. The cleaned RH was then dried overnight in an oven at 100ºC followed by treating with 0.2 M H_2SO_4 (acid to RH ratio was 10 L/kg) at 100ºC for 2 hrs. After cooling and filtering, the RH was washed with copious amount of water to remove any trace of sulphuric acid and finally dried at 100 ºC [1]. Entire processing steps resulted about 40% weight loss of RH. On the other hand, collected ES was washed thoroughly with tap water. Then the inner shell membrane was removed from ES and boiled in water for 30 min. Finally, the boiled ES was dried at 100 ºC [2].

Synthesis of wollastonite by indirect method

In order to synthesize wollastonite using RH and ES as the starting materials, at first an indirect calcination method [21] was followed which was then scaled up by developing the direct sintering approach. Since theoretically the wt% of CaO and SiO_2 in wollastonite is 48% and 52% respectively [1-2], so to determine the exact wt.% of CaO and SiO_2 in ES and RH our primary attempt was confined with the indirect method as adopted by Hossain et al. [21]. In the indirect method, SiO_2 was extracted from treated RH following the previously described methods [1,21] but extending the calcination temperature up to 1,000 ºC. On the other hand, 3 hours thermal treatment (at 1,000 ºC) of ES resulted the formation of CaO [21]. Then stoichiometric amount of CaO and SiO_2 were mixed homogeneously for 30 minutes at 1,000 rpm using a high-energy ball mill (Model: MSK-SFM-1 QM 3SP2) followed by thermal treatment at 1,000 ºC for 3 hrs. which facilitated the formation of desired wollastonite.

Synthesis of wollastonite by direct calcination of RH and ES

In the direct method, a series of ratio of powdered RH and ES (10:2.6, 10:3.0, 10:3.3 and 10:3.7) were chosen as the starting materials and each selected proportion was straightaway ball milled for 30 minutes at 1,000 rpm to get the mixture in homogeneous form. Then the desired wollastonite was produced by sintering the mixture in a muffle furnace at 1,000 ºC

for 3 hrs. The schematic representations of the indirect and direct synthesis process are displayed in Fig. 1.

Characterization of synthesized wollastonite

Synthesized wollastonite was characterized by various techniques e.g. X-ray diffractometer (XRD), Fourier transform infrared spectrophotometer (FT-IR), Scanning electron microscopy (SEM) and Thermogravimetric (TG/DTA) analyses.

The respective phases of wollastonite were identified by the XRD (PANalytical X'Pert PRO XRD PW 3040). Intensity data were collected by fixing scanning range, $2\theta = 10^{o} - 75^{o}$ using Cu $K\alpha$ radiation ($\lambda = 1.5406$ Å) with a step scan of 4°/min. To confirm the presence of desired phases, recorded data were compared with standard JCPDS files.

The presence of the functional group was explored by recording the FT-IR spectrum using (Prestige 21; SHIMADZU) a FT-IR spectrophotometer. The sample-to-KBr ratio was 1:100 while the scanning range was 4000 to 400 cm^{-1} and the resolution was 4 cm^{-1} with 32 scanning.

The thermogravimetric analysis (TGA) was carried out on an EXSTAR TG/DTA 6300 with alpha-alumina powder as a reference sample from 30 to 1,000 °C in nitrogen atmosphere (flow rate 50 nmL/min). The heating rate was 20 °C/min. The surface morphology and microstructural features of the synthesized material were observed by SEM (Phenom Pro) applying an accelerating voltage of 15 kV.

Bioactivity studies

In-vitro bioactivity response is the evaluation of apatite-forming ability (mainly hydroxyapatite, HAp), on the surface of bio-material in simulated body fluid (SBF). A previously published method [1] was followed for this purpose. About 0.2 g of synthesized wollastonite powder was immersed into 30 ml SBF at 37 °C. The growth of HAp was monitored at different time intervals (1, 3 and 7 days). To investigate the formation of HAp on the surface of wollastonite powder, first the SBF solution was drained out carefully then the powder was gently rinsed with deionized water to remove excess SBF followed by drying at 50 °C. The formation of apatite layers was examined by XRD and SEM.

Results and Discussion

XRD analysis

Given in Fig. 2 is the x-ray diffratogram of as received

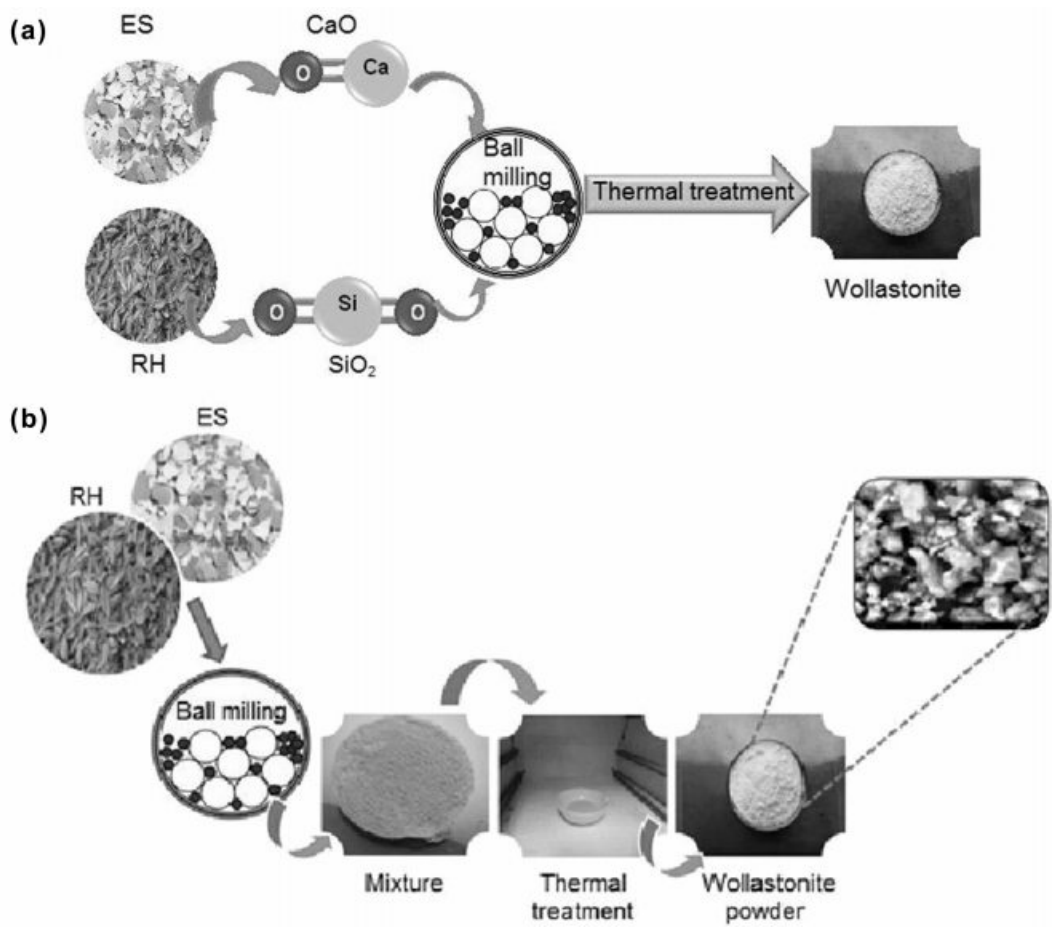

Fig. 1. Schematic representation of the synthesis of wollastonite (a) Indirect method, (b) Direct method.

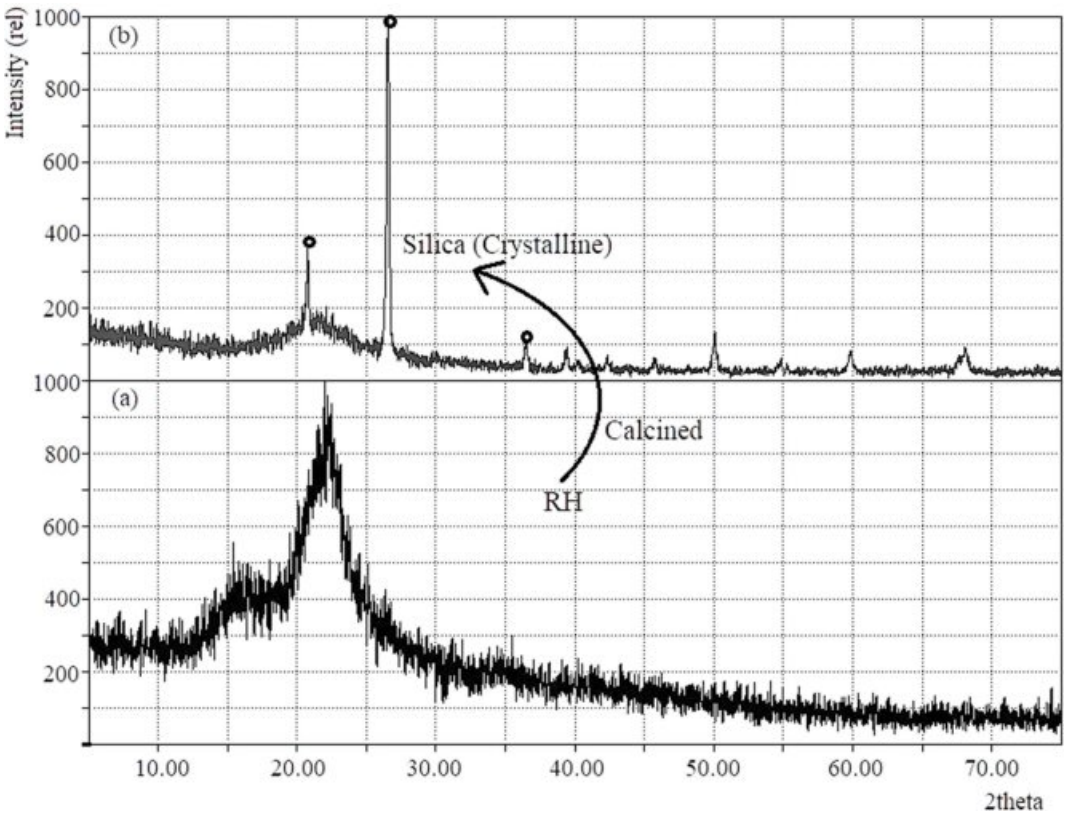

Fig. 2. XRD pattern of (a) treated RH and (b) silica obtained from RH treated at 1,000 °C.

RH and after calcination at 1,000 °C. The XRD pattern of SiO_2 (Fig. 2b) having 2θ values of 21.9°, 26.6° and 36.0° indicates that the silica formed in crystalline nature as expected. Because, it is well known that the presence of amorphous silica, crystalline silica or both phases strictly depends on the calcination temperature [41, 42]. The characteristic peaks of tridymite (2θ = 21.6°) and cristobalite (2θ = 21.8°) phases coincides giving a single peak at 21.9°. This could be due to the melting of the surfaces of ash silica particles followed by formation of bonding of the particles together [41, 42].

The XRD patterns of the ES before and after calcination are displayed in Fig. 3(a, b). It is apparent from the recorded diffraction data (Fig. 3a) that the ES without being thermally treated shows the usual characteristic peaks for rhombohedral calcite (File # 5-0586). The characteristic peak detected at 2θ position 29.485° (1 0 4) plane coupled with several peaks at 23.07°, 36.06°, 39.48°, 43.26°, 47.64° and 48.6° confirmed the mineral phase of egg shell as calcite and no other crystalline phase was observed.

Conversely, after calcination (Fig. 3b) of ES, existence of the distinctive peak at 2θ position 37.09° (2 0 0) plane supports the formation of CaO. Moreover, the calcined sample showed no peak at 2θ = 29.48° which indicates that $CaCO_3$ has completely changed to CaO [43].

However, the total percentage of silica (SiO_2) and CaO formed due to calcination of RH and ES at 1,000 °C were found to be 20% and 55% respectively. Following earlier studies [14, 15, 19], our indirect approach used an equal ratio of these two calcined products (i.e. CaO and SiO_2) to synthesize wollastonite. But as our intention was to investigate the impact of the ratio of RH and ES on the direct synthesis of wollastonite, we explored a facile pathway where blend of RH and ES (at different ratios, 10:3.7; 10:3.3; 10:3.0 and 10:2.6) were straight away calcined to get the desired wollastonite. Fig. 4 demonstrates the corresponding x-ray diffractograms of wollastonite as synthesized using the above-mentioned ratios of RH and ES. It is clearly evident from Fig. 4 that the initial ratio of RH and ES plays a key role in controlling the formation of wollastonite as the major phase. Although the four chosen proportions of RH and ES effectively produced wollastonite (consistent with the JCPDS file no. 043-1460) [10] but together with wollastonite, larnite (Ca_2SiO_4) as well as unreacted CaO and SiO_2 were also indexed [13]. The wollastonite phase (ICDD number: 00-043-1460) [10, 31] was recorded in Fig. 4(a-d) at 2 theta positions 23.1, 25.4, 26.9, 28.9, 30.0, 36.2, 38.2, 39.2, 41.3 showed a good match with previous investigations [10, 31] while calculated lattice parameters (a = 15·46, b = 7·33 and c = 7·19 Å) were also found to be in good agreement [10, 31].

Obviously, the formation of wollastonite with mixed

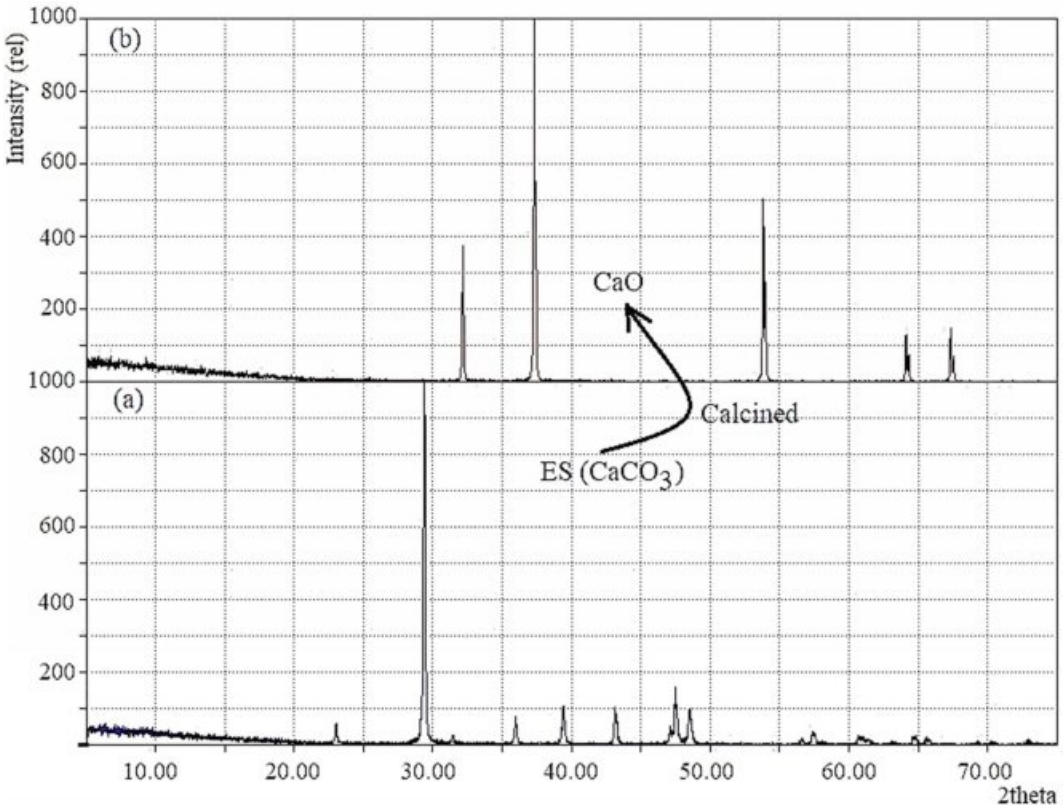

Fig. 3. XRD pattern of (a) ES and (b) CaO obtained from ES treated at 1,000 ºC.

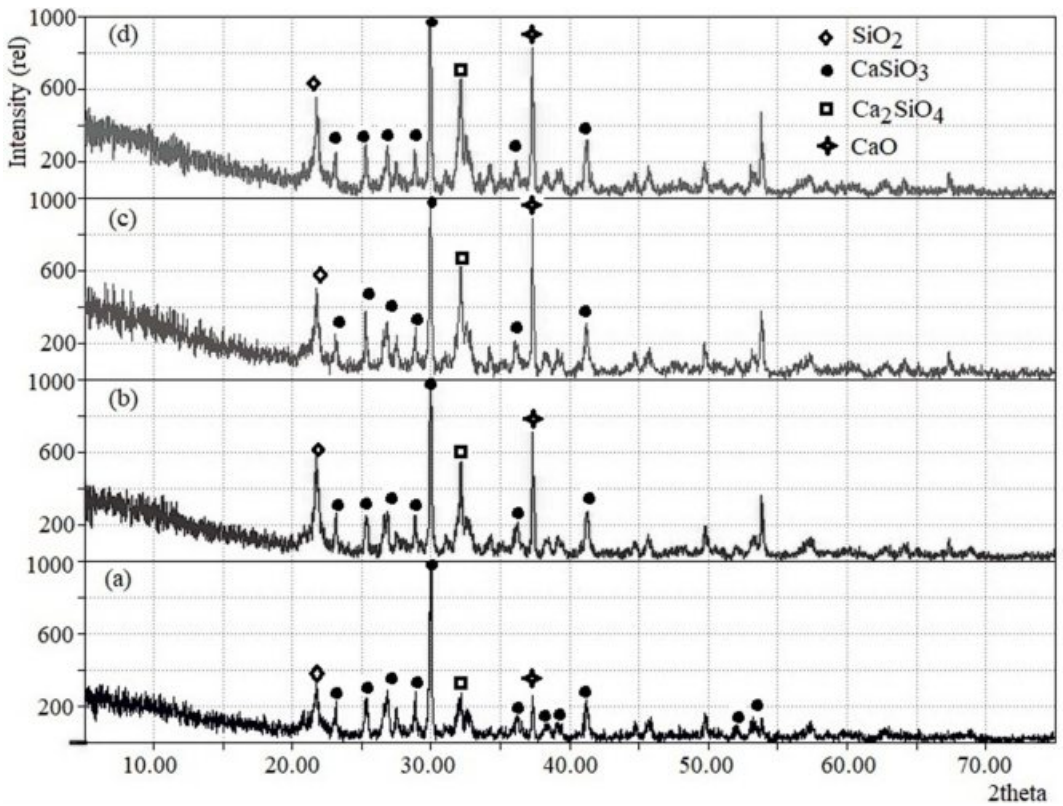

Fig. 4. XRD pattern of RH-ES powders calcined at 1,000 ºC. RH:ES = (a) 10:2.6. (b) 10:3.0. (c) 10:3.3 and (d) 10:3.7.

phases strictly depends on the fraction of RH and ES used. The characteristic peaks for CaO, SiO_2 and larnite were very prominent (as shown in Fig. 4b, 4c and 4d) when the ratios of RH and ES were 10:3.0, 10:3.3 and 10:3.7. On the other hand, these three peaks appeared in suppressed state making the wollastonite phase as predominant when the RH:ES ratio was fixed at 10:2.6 (Fig. 4a). As it has been observed from the XRD data that among the four combinations of RH to ES ratios, better result was obtained at RH:ES ratio 10:2.6, we further proceeded with the FT-IR analysis of wollastonite synthesized using this ratio of RH:ES.

FT-IR analysis

Fig. 5 represents a typical FT-IR spectrum of the synthesized wollastonite. Recorded FT-IR band positions as tabulated in Table 2, were fairly consistent with previous studies [6, 10, 14]. Noticeably, the band position observed around 476 cm^{-1} represents the vibrational bending mode of Si – O – Si bond while the vibrational stretching mode of O – Si – O bond is positioned at 792.74 cm^{-1}. Si – O –Ca bond having ion-bridging oxygen is noticed at band positions 905-945 cm^{-1}. Vibrational stretching mode of Si–O–Si bond was observed in the range of 1,014 to 1,091 cm^{-1}. The bands around 1,639 and 3,400 cm^{-1} are responsible for the moisture content present in the sample.

Thermogravimetry analysis

Since the RH and ES mixture of 10:2.6 ratio was the best combination for synthesizing wollastonite by direct calcination, further investigation was focused on the thermogravimetric analysis of this mixture in raw state (i.e. without calcination). Given in Fig. 6 are the TG and DTG behavior of RH and ES (10:2.6) blend which can be described consequently depending on different stages. It is apparent from the Fig. 6 that there are three visible endothermic peaks at 65, 378 and 745 ºC. The first weight loss (~4%), as shown in TGA starts from ambient temperature to 65 ºC, is responsible for the release of the moisture from the sample during heating. The major decomposition occurred at 378 ºC where approximately 47% weight was lost. This is due to the degradation of chemically bound water, cellulose,

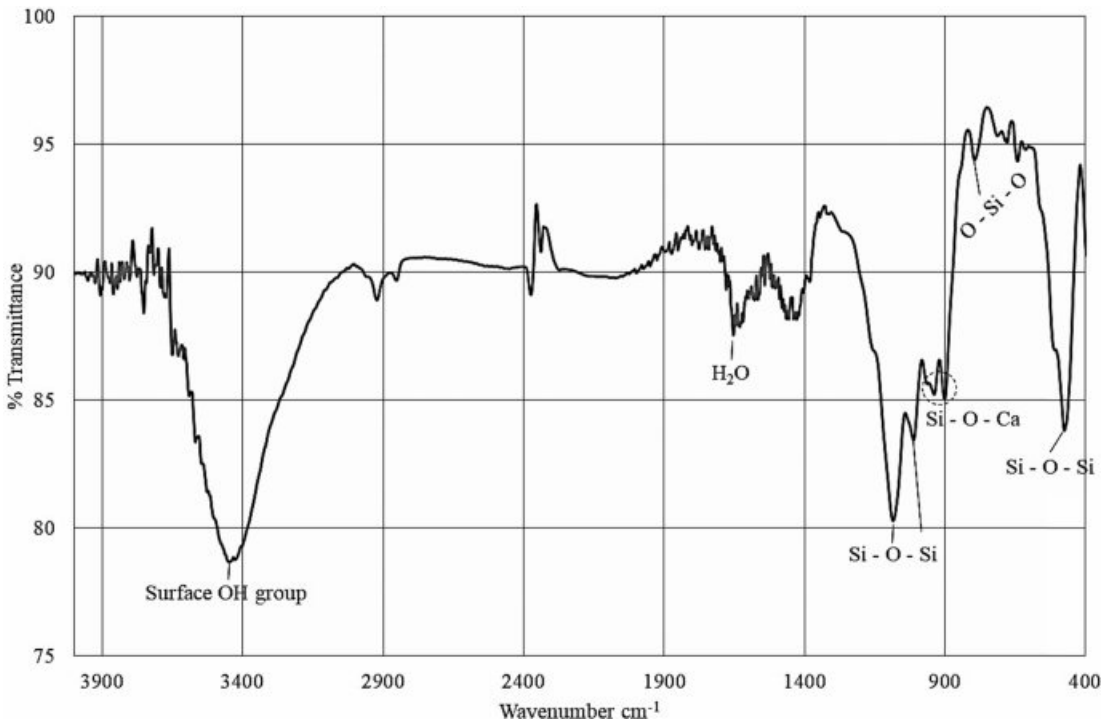

Fig. 5. FT-IR spectrum of the wollastonite synthesized by calcining the mixture of RH and ES (ratio = 10:2.6) at 1,000 ºC for 3 hrs.

Table 2. FT-IR band positions of wollastonite synthesized at RH:ES ratio 10:2.6.

Band positions, cm^{-1}	Corresponding assignments
474.49	Vibrational bending of Si – O – Si and O – Si – O
794.67	Vibrational stretching of O – Si – O
905.62, 945.12	Si – O –Ca bonds comprising ion-bridging oxygen
1014.56, 1085.92	Vibrational stretching of Si – O – Si
1651.07	Bending vibration of H_2O
3448.72	Absorption of moisture on the surface of wollastonite

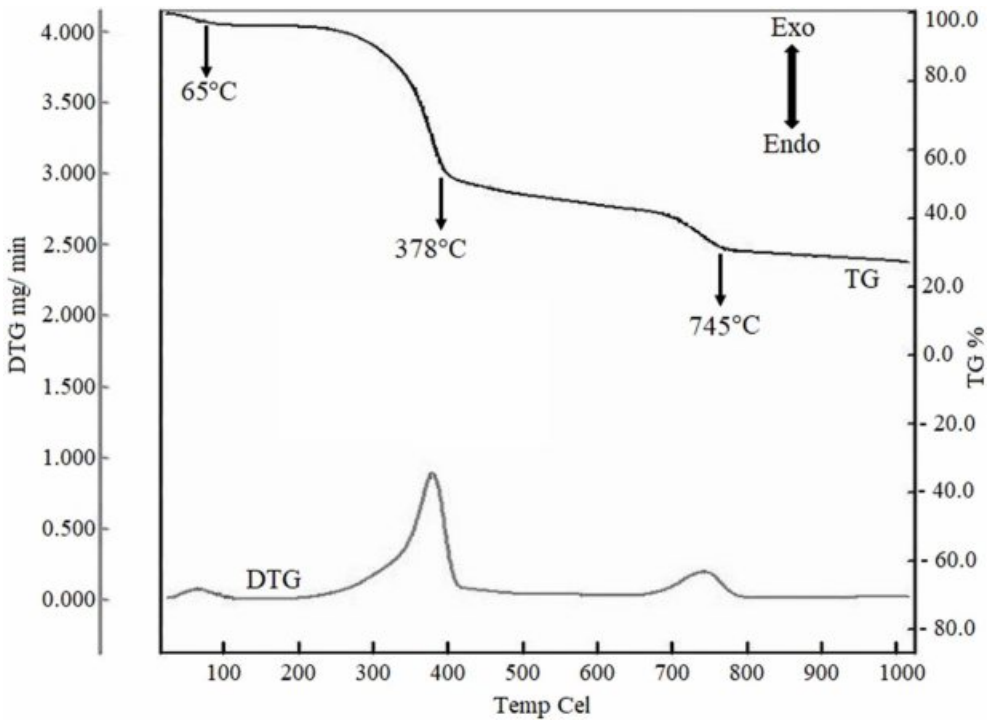

Fig. 6. TGA and DTG representation for the TGA for RH and ES (10:2.6) mixture

hemicelluloses and lignin from RH [44]. Finally, an endothermic peak at 745 ºC is due to high-temperature decarbonation i.e. due to the decomposition of calcium carbonate from ES according to the reaction (1) [45]. The weight was constant after 800 ºC. Observed TG profile is in line with many previous studies where such three steps weight loss behaviour was well documented [33, 46-48].

$$CaCO_3(\text{eggshell}) \rightarrow CaO + CO_2\uparrow \quad (1)$$

No significant weight change was observed in TG curve after 800 ºC. Surprisingly, the DTG curve also featured three exothermic peaks at 65, 378 and 745 ºC. The exothermic hump at 65 ºC could be the representative for the elimination of physically adsorbed humidity water. The 2nd exothermic signal at 378 ºC is comparatively strong than the other two exothermic peaks. This is probably due to the burning of organic matter from ES and RH [21]. The 3rd exothermic peak recorded at around 750 ºC could be due to the formation of $CaSi_2O_4$ and $CaSiO_3$ crystalline phases [13]. It should be mentioned here that Sreekanth et al. [48] also obtained an exothermic peak of the DTA at 890 ºC, which is the preparatory temperature for the crystallization of $CaSiO_3$.

In-vitro Bioactivity Response of wollastonite synthesized using RH:ES ratio 10:2.6

The wt % ratio of RH and ES appeared significant in producing the desired wollastonite. When the combinations of RH and ES were 10:3.0, 10:3.3 and 10:3.7, formation of larnite (Ca_2SiO_4) became significant with wollastonite. Additionally, CaO and SiO_2 were also present with the desired product. On the other hand, formation of wollastonite as major phase was visualized when the RH:ES ratio was fixed at 10:2.6 while larnite formation was suppressed. Since, wollastonite shows high biocompatibility as compared to other silicate based ceramics, so it is presumed that wollastonite synthesized using this optimum ratio will show better bioactive properties as larnite formation was suppressed in this case. However, further investigation in this direction is yet to be explored.

SEM images of wollastonite powder showing the in-vitro bioactivity response i.e. the apatite forming ability are depicted in Fig. 7(a-d). Fig. 7(a) illustrates the surface morphology of bare wollastonite which is in agglomerated form. However, in comparison with this sample, it is clearly evident from Fig. 7(b, c, d) that as a result of immersing in SBF the surface of wollastonite samples come to be covered by newly formed apatite (HAp) layers and a continuous deposit of dense apatite takes place with time. This was further validated by XRD data. The stacked XRD diffractograms of wollastonite before and after soaking in SBF are shown in Fig. 8. In SBF treated wollastonite, coupled with wollastonite peak, the characteristic peak of HAp representing the (2 1 1) plane is also detected at 2θ position 31.79º and this observation is in good agreement with earlier studies [11,49]. Supporting the SEM observation, it is evident that as more and more apatite forms, intensity

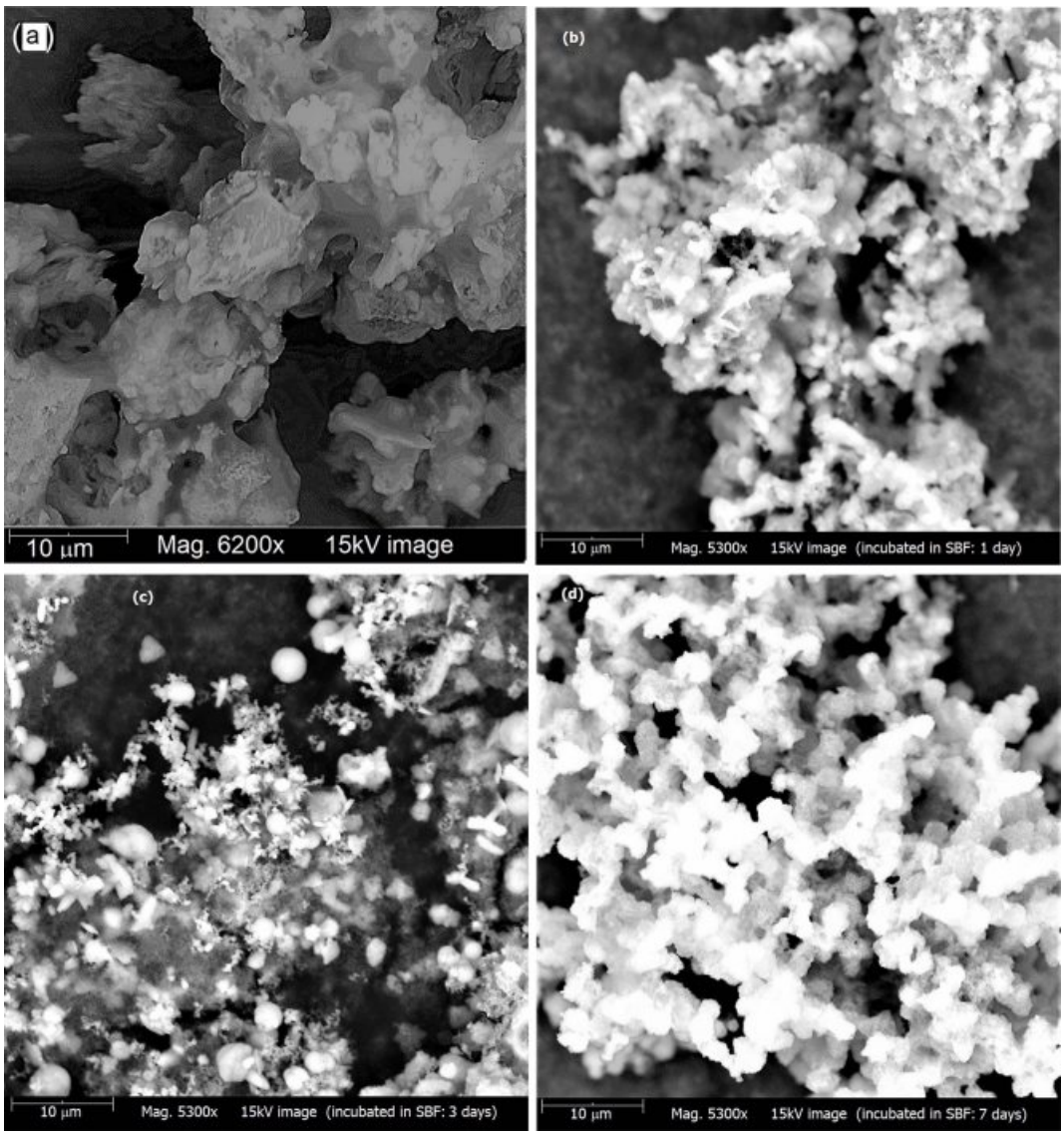

Fig. 7. SEM images of (a) bare wollastonite samples and (b, c, d) after soaking in SBF for 1, 3 and 7 days respectively

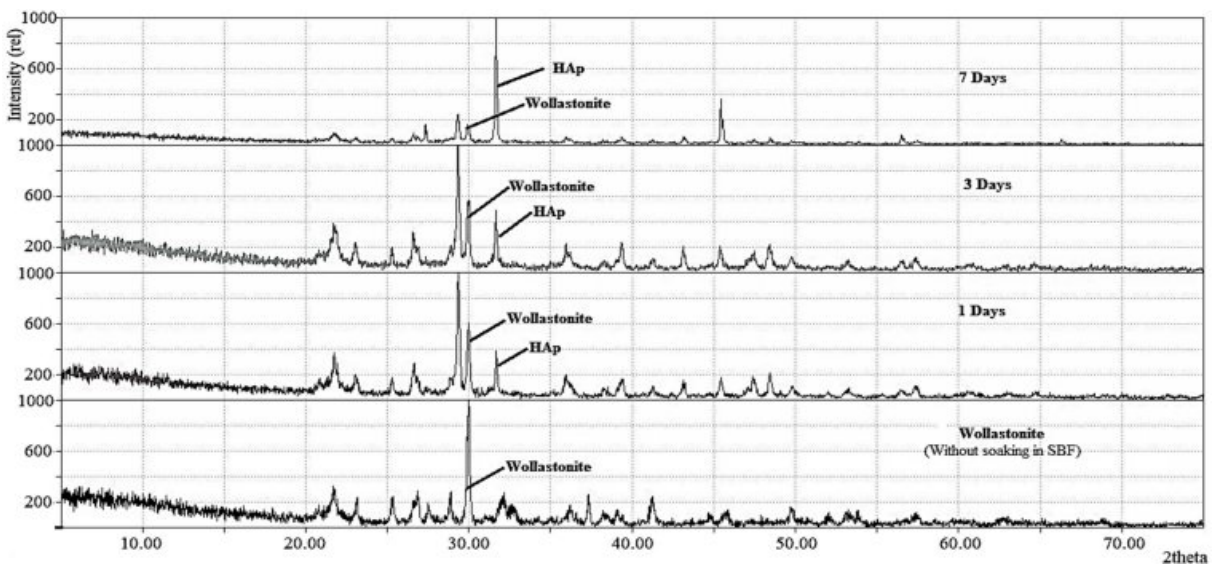

Fig. 8. XRD diffractograms of bare wollastonite samples and after soaking in SBF for 1, 3 and 7 days.

of this freshly formed peak goes toward the upward direction with the course of time. On the other hand, the intensity of wollastonite peak gradually declines. This result supports that the wollastonite synthesized by thermal treatment of two waste materials e.g. RH and ES shows bioactive properties by inducing direct bone ingrowth while incubated in physiological environment.

Mechanism of HAp formation

The bioactive response of wollastonite is accredited to the nucleation of hydroxyapatite (HAp) and this phenomenon becomes activated by the dissolution of calcium and silicate ions. Hence, the mechanism of HAp formation on the surface of wollastonite powder soaked in SBF can be elucidated following previous studies [6, 15, 49, 50]. Briefly, according to Equation 2, due to immersion in SBF, Ca^{2+} present in wollastonite tends to exchange with existing H^+ of SBF forming silanol (Si – OH) in the surface layer. This process increases the pH at wollastonite-SBF interface and consequently a negatively charged surface having functional group (Si – O^-) is formed (Equation 3). The Ca^{2+} ions present in SBF solution are firstly attracted to the solid - liquid interface which causes the ionic activity product (IP) of apatite to be high enough at the interface. Such an environment favours the growth of apatite on wollastonite surface. Once the apatite begins nucleation, spontaneous growth occurs with the aid of calcium and phosphate ion consumption from the mother SBF solution (Equation 4). Fig. 9 depicts the pictorial representation of HAp formation mechanism on wollastonite surface.

$$\equiv Si - O - Ca - O - Si + H^+ \rightarrow \equiv Si - OH + Ca^{2+} \quad (2)$$

$$\equiv Si - OH + OH \rightarrow Si - O^- + H_2O \quad (3)$$

$$Ca^{2+} + HPO_4^{2-} \rightarrow Ca_{10}(PO_4)_6(OH)_2 \quad (4)$$

Conclusion

The research work reported here in particular demonstrated the influence of initial ratio of the raw materials, RH and ES in synthesizing wollastonite directly by solid state method. Although different combinations of the starting materials have been used by different researchers, but effect of the ratio of ES and RH has not been explored yet. Hence the purpose of this research work was to develop a protocol to synthesize wollastonite from RH and ES and to the best of our knowledge, for the first time we have investigated such effect on the formation of wollastonite using RH and ES. Our approach revealed that the initial ratio of RH and ES plays a key role in controlling the formation of wollastonite as the major phase. The optimum ratio

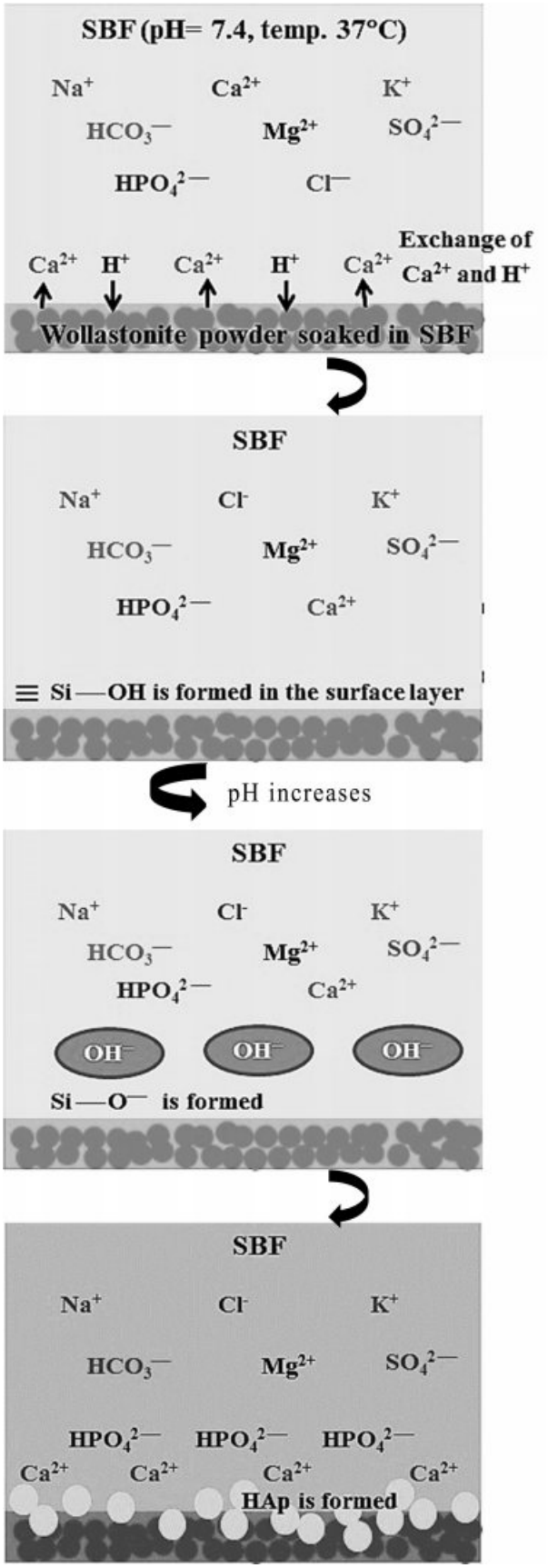

Fig. 9. Schematic representation of apatite formation on wollastonite surface in SBF.

of RH: ES to synthesize wollastonite as the major phase was found to be 10:2.6 which was confirmed by x-ray diffraction (XRD) and Fourier Transform Infrared (FT-IR) techniques. Moreover, the bioactive response of the wollastonite synthesized using above mentioned ratio of RH:ES showed excellent in-vitro bioactive properties. Such observation revealed its suitability to be used as biomaterials.

Since, it is well-known that fine particles of the ingredients speed up the diffusion reaction for the phase transition during calcination and also helps to get the product in pure form thus further advancement of our research focuses on investigating the effect of particle size (ranging from fine to course) of the raw materials in synthesizing wollastonite.

Acknowledgement

This research work was supported by BCSIR through R&D project (Ref. 39.02.0000.11.014.007.2017/848, Dated 26/09/2017). Sazia Sultana and Md. Maksudur Rahman also acknowledges BCSIR for 'Nurul Abser Khan' Post Graduate Fellowship. Thanks to Dr. M. A. Gafur, Principal Scientific Officer, Pilot Plant & Process Development Centre, BCSIR, Dhaka for providing TGA facilities.

References

1. S. Ke, X. Cheng, Y. Wang, Q. Wang, and H. Wang, Ceram. Int. 39[5] (2013) 4953-4960.
2. M. Felipe-Sesé, D. Eliche-Quesada, and F.A. Corpas-Iglesias, Ceram. Int. 37[8] (2011) 3019-3028.
3. P. Kalla, A. Misra, R.C. Gupta, L. Csetenyi, V. Gahlot, and A. Arora, Constr. Build. Mater. 40 (2013) 1142-1150.
4. M.R.F. Gonçalves, C.K. Fillipeto, J. Vicenzi, and C.P. Bergmann, Constr. Build. Mater. 25[1] (2011) 320-327.
5. M. Mehrali, S.F.S. Shirazi, S. Baradaran, M. Mehrali, H.S.C. Metselaar, N.A.B. Kadri, and N.A.A. Osman, Ultrasonics Sonochemistry 21[2] (2014) 735-742.
6. A. Udduttula, S. Koppala, and S. Swamiappan, Trans. Ind. Ceram. Soc. 72[4] (2013) 257-260.
7. H. Begam, S. Mandal, J. Mukherjee, and S. K. Nandi, Trans. Ind. Ceram. Soc. 73[4] (2014) 284-292.
8. K. Maji and S. Dasgupta, Trans. Ind. Ceram. Soc. 73[2] (2014) 110-114.
9. R. Lakshmi, V. Velmurugan, and S. Sasikumar, Combust. Sci. Technol. 185[12] (2013) 1777-1785.
10. U. Anjaneyulu and S. Sasikumar, Bull. Mater. Sci. 37[2] (2014) 207-212.
11. R. Morsy, R. Abuelkhair, and T. Elnimr, Silicon 9[4] (2017) 489-493.
12. R. Morsy, R. Abuelkhair, and T. Elnimr, Silicon 9[4] (2017) 637-641.
13. H. Wang, Q. Zhang, H. Yang, and H. Sun, Ceram. Intl. 34[6] (2008) 1405-1408.
14. N. Tangboriboon, T. Khongnakhon, S. Kittikul, R. Kunanuruksapong, and A. Sirivat, J. Sol-Gel Sci. Technol. 58[1] (2011) 33-41.
15. H. Ismail, R. Shamsudin, M.A.A. Hamid, and R. Awang, J. Aust. Ceram. Soc. 52[2] (2016) 163-174.
16. R. Puntharod, C. Sankram, N. Chantaramee, P. Pookmanee, and K.J. Haller, J. Ceram. Proc. Res. 14[2] (2013) 198-201.
17. K. Yanagisawa, X. Hu, A. Onda, and K. Kajiyoshi, Cement and Concrete Research, 36[5] (2006) 810-816.
18. A.Yazdani, H.R. Rezaie, H. Ghassai, and M. Mahmoudian, J. Ceram. Proces. Res. 14[1] (2013) 12-16.
19. R. Phuttawong, N. Chantaramee, P. Pookmanee, and R. Puntharod, Adv. Mater. Res. 1103 (2015) 1-7.
20. S. Chehhlatt, A. Harabi, H. Oudadesse, and E. Harabi, Acta Physica Polonica A 127[4] (2015) 925-927.
21. S. S. Hossain and P. K. Roy, J. Asian Ceram. Soc. 6[3] (2018) 289-298.
22. S. Vichaphund, M. Kitiwan, D. Atong, and P. Thavorniti, J. Euro. Ceram. Soc. 31[14] (2011) 2435-2440.
23. K. Xiong, H. Shi, J. Q. Liu, Z. Shen, H. Li, and J. Ye, J. Am. Ceram. Soc. 96[3] (2013) 691-696.
24. S. Palakurthy, K.V. Reddy, R.K. Samudrala, and P.A. Azeem, Mat. Sci. and Eng. C 98 (2019) 109-117.
25. S. Palakurthy, P.A. Azeem, and K.V. Reddy, Ceramics International Part B 45[18] (2019) 25044-25051.
26. F.A.A. Azam, R. Shamsudin, M.H. Ng, A. Ahmad, M.A.M. Akbar, and Z. Rashidbenam, Ceramics International 44[10] (2018) 11381-11389.
27. A.P. Solonenko, A.I. Blesman, and D.A. Polonyankin, Ceramics International 44[18] (2018) 17824-17834.
28. I.V. de S.R. Nascimento, W.T. Barbosa, R.G. Carrodeguas, M.V.L. Fook, and M.A. Rodŕıguez, International Journal of Chemical Engineering, Article ID 6213568 (2018) 1-8.
29. L.A. Adams, E.R. Essien, and E.E. Kaufmann, J. Asian Ceram. Soc. 6[2] (2018) 132-138.
30. Heriyanto, F. Pahlevani, and V. Sahajwalla, J. Cleaner Production. 172 (2018) 3019-3027.
31. R. Shamsudin, F.A.A. Azam, M.A.A. Hamid, and H. Ismail, Materials 10[10] (2017) 1188.
32. K.A. Almasri, Hj. Ab A. Sidek, K.A. Matori, and M.H.M. Zaid, Results in Physics 7 (2017) 2242-2247.
33. H. Ismail, R. Shamsudin, and M.A.A. Hamid, Mat. Sci. and Eng. C 58 (2016) 1077-1081.
34. E.K. Papynov, O.O. Shichalin, E.B. Modin, V. Yu. Mayorov, A.S. Portnyagin, S.P. Kobylyakov, A.V. Golub, M.A. Medkov, I.G. Tananaev, and V.A. Avramenko, RSC Adv. 6[40] (2016) 34066-34073.
35. R. Shamsudin, M.A.A. Hamid, and A. Jalar, J. Asian Ceram. Soc. 2[1] (2014) 77-81.
36. A. Yazdani, H.R. Rezaie, and H. Ghassai, J. Ceram. Proc. Res. 11[3] (2010) 348-353.
37. D. Battegazzore, S. Bocchini, J. Alongia, and A. Frachea, RSC Adv. 4[97] (2014) 54703-54712.
38. S. Ahmed, F. Nigar, A.I. Mustafa, and M. Ahsan, Trans. Ind. Ceram. Soc. 76[4] (2017) 215-221.
39. S.J. Nipa and M.A. Hossain, Intl. J. Sci. & Engg. Res. 6[10] (2015) 387-391.
40. M.A. Hamid, M.A. Rahman, S. Ahmed, and K.M. Hossain, Asian J. Poult. Sci. 11[1] (2017) 1-13.
41. Y. Shinohara and N. Kohyama, Industrial Health 42[2] (2004) 277-285.
42. J.F. Saceda, R.L. de Leon, K. Rintramee, S. Prayoonpokarach, and J. Wittayakun, Quim. Nova 34[8] (2011) 1394-1397.
43. E.M. Rivera, M. Araiza, W. Brostow, V.M. Castaño, J.R. Díaz-Estrada, R. Hernández, and J.R. Rudriguez, Mat. Lett. 41[3] (1999) 128-134.
44. P.M.K. Reddy, S. Mahammadunnisa, B. Ramaraju, B. Sreedhar, and C. Subrahmanyam, Environ. Sci. and Poll. Res. 20[6] (2013) 4111-4124.
45. M.N. Freire and J.N.F. Holanda, Ceramica 52[324] (2006)

240-244.
46. D.S. Klimesch and A. Ray, Thermochimica Acta 306[1-2] (1997) 159-165.
47. R.P. S. Chakradhar, B.M. Nagabhushana, G.T. Chandrappa, K.P. Ramesha, and J.L. Rao, Materials Chemistry and Physics 95[1] (2006) 169-175.
48. S.K.S. Hossain and P.K. Roy, Boletín de la Sociedad Española de Cerámica y Vidrio 58[3] (2019) 115-125.
49. A. Harabi and S. Chehlatt, J. Therm. Anal. Calorim. 111[1] (2013) 203-211.
50. X. Liu, C. Ding, and P.K. Chu, Biomaterials 25[10] (2004) 1755-1761.